Available online at www.sciencedirect.com
ScienceDirect
Journal of Catalysis 250 (2007) 55–66
JOURNAL OF CATALYSIS
www.elsevier.com/locate/jcat

# The role of alumina in the supported Mo/HBeta–$Al_2O_3$ catalyst for olefin metathesis: A high-resolution solid-state NMR and electron microscopy study

Xiujie Li, Weiping Zhang *, Shenglin Liu, Longya Xu, Xiuwen Han, Xinhe Bao *

*State Key Laboratory of Catalysis, Dalian Institute of Chemical Physics, Chinese Academy of Sciences, 457 Zhongshan Road, Dalian 116023, China*

Received 5 February 2007; revised 25 May 2007; accepted 28 May 2007

Available online 28 June 2007

**Abstract**

High-resolution solid-state MAS NMR; hyperpolarized $^{129}$Xe NMR, SEM, and TEM; XRD; and $N_2$ adsorption were used to investigate the role of alumina in the Mo/HBeta–$Al_2O_3$ catalyst. XRD and $N_2$ adsorption showed that introduction of alumina into the support may protect the HBeta framework from destruction. Quantitative $^{29}$Si MAS, $^{27}$Al MAS, and MQ MAS NMR spectra demonstrated that dealumination occurs preferentially at specific T-sites in the Mo/HBeta catalyst; however, the framework aluminum in HBeta zeolites remains at the same crystallographic sites after the addition of alumina. Hyperpolarized $^{129}$Xe NMR, HRTEM, and SEM images indicate that Mo species are readily dispersed in alumina rather than in HBeta zeolites. The preferential migration of Mo species into the alumina pores may preserve the integrity of the HBeta zeolite framework and result in the moderate distribution of Mo species and acidity in the composite support. These may be correlated with the high performance of Mo/HBeta–$Al_2O_3$ catalysts in the metathesis of ethene and butene-2 to propene.


*Keywords:* Olefin metathesis; Mo/HBeta–$Al_2O_3$ catalyst; Solid-state NMR; $^{27}$Al MQ MAS NMR; Hyperpolarized $^{129}$Xe NMR; Electron microscopy

## 1. Introduction

Olefin metathesis has received increasing attention and is now considered one of the most important C–C bond formation reactions [1–3]. Chauvin, Grubbs, and Schrock won the Nobel Prize in chemistry in 2005 for their development of the olefin metathesis in homogeneous systems. Heterogeneous catalysts for metathesis reactions are of further interest due to their ease of separation, good persistence, and recyclability [4,5]. A number of solid catalysts have been reported for the olefin metathesis, the most feasible of which are those based on Re, W, and Mo [6–16]. Of these, supported $Re_2O_7/Al_2O_3$ is highly active and selective even at room temperature, and its catalytic performance can be improved by using composite supports, such as $Al_2O_3$–$SiO_2$ [9], $Al_2O_3$–$B_2O_3$ [10,11], and $Al_2O_3$–$P_2O_5$ [12]. However, rhenium oxide will sublime when calcined [13], which may restrict its range of practical applications. The supported tungsten oxide catalysts are less active and require much higher reaction temperatures (523–773 K) to achieve considerable metathesis activity [14,15]. Recently, our laboratory reported that Mo supported on HBeta–$Al_2O_3$ composites exhibited high activity in the metathesis of ethene and butene-2 to propene at ca. 393 K, which offers an alternative pathway for the production of propene [16]. In contrast, Mo supported on HBeta zeolites performed poorly due to the strong interaction between Mo species and HBeta zeolites [17]. Thus, the composition and structure of the support play an important role in the heterogeneous olefin metathesis reaction. In this work, we demonstrate the importance of choosing a suitable support for optimizing the propene production. The role of alumina in the composite support have been revealed by $^{29}$Si MAS NMR, $^{27}$Al MAS NMR, two-dimensional $^{27}$Al 3Q MAS NMR, $N_2$ adsorption, hyperpolarized $^{129}$Xe NMR, high-resolution SEM, and TEM. The varying distributions of Mo species in the HBeta and alumina composite support have been demonstrated. These may be correlated with the high catalytic

* Corresponding authors. Fax: +86 411 8469 4447.
*E-mail addresses:* wpzhang@dicp.ac.cn (W. Zhang), xhbao@dicp.ac.cn (X. Bao).

0021-9517/$ – see front matter 
doi:10.1016/j.jcat.2007.05.019

performance of Mo/HBeta–$Al_2O_3$ in the metathesis of ethene and butene-2 to propene.

## 2. Experimental

### 2.1. Catalyst preparation

The HBeta and $\gamma$-$Al_2O_3$ composite support was prepared by extruding a mixture of $\gamma$-$Al_2O_3$ and HBeta zeolite (Si/Al = 15 provided by Fushun Petroleum Company, China) powder into strips of ca. 2 mm diameter. The supports, designated HB-$n$Al, were then calcined at 773 K for 2 h and ground to 16–32 mesh. Catalysts containing ca. 4.0 wt% Mo were prepared by wet impregnation of HBeta–$Al_2O_3$ strips with an aqueous solution of $(NH_4)_6Mo_7O_{24}{\cdot}4H_2O$, then dried at 393 K, and finally calcined at 953 K for 2 h. The catalysts are designated 4Mo/HB-$n$Al, where $n$ (%) represents the weight percent of $\gamma$-$Al_2O_3$ in the support.

### 2.2. Catalyst characterization

#### 2.2.1. XRD, $N_2$ adsorption, SEM, and TEM measurements

XRD patterns were obtained at room temperature on a Rigaku D/Max-RB diffractometer using Cu$K\alpha$ radiation. Powder diffractograms of samples were recorded over a range of $2\theta$ values from 5° to 50° at 40 kV and 100 mA with a scanning rate of 8 deg/min. The integrated intensity of the signal at $2\theta = 22.4°$ was used to evaluate the crystallinity of the Beta zeolites. Nitrogen sorption experiments were performed at 77 K on an ASAP 2000 system in the static measurement mode. Samples were degassed at 623 K for 10 h before the measurements. Specific surface areas were calculated by the BET method, and the pore volume was determined by $N_2$ adsorption at a relative pressure of 0.98. SEM images were obtained using a Hitachi S4800 field-emission microscope. TEM images were obtained with a Philips CM 200 microscope equipped with a CCD camera at an acceleration voltage of 200 kV. Energy-dispersive spectroscopy (EDS) analysis also was done using this microscope equipped with an X-ray energy analyzer.

#### 2.2.2. MAS NMR measurements

All NMR spectra were recorded on Varian Infinityplus-400 spectrometer. $^{27}$Al MAS NMR experiments were carried out at 104.2 MHz using a 4-mm MAS NMR probe with a spinning rate of 15 kHz. Chemical shifts were referenced to $(NH_4)Al(SO_4)_2{\cdot}12H_2O$ at −0.4 ppm as a secondary reference. The spectra were accumulated for 1024 scans with a $\pi/12$ flip angle and 2-s pulse delay. For a quantitative comparison, all samples were weighted and hydrated completely in a desiccator with saturated $NH_4NO_3$ solution, and the spectra were calibrated by measuring a known amount of $(NH_4)Al(SO_4)_2{\cdot}12H_2O$ under the same NMR acquisition conditions [18,19]. $^{27}$Al 3Q MAS NMR experiments were performed using a three-pulse sequence incorporating a $z$-filter at a spinning speed of 25 kHz with a 2.5-mm probe [20]. An rf field of 200 kHz was used for the creation ($0Q \rightarrow \pm 3Q$) and the first conversion ($\pm 3Q \rightarrow 0Q$) pulses. An rf field of 18 kHz was used for the last conversion step ($0Q \rightarrow \pm 1Q$), which was the central transition selective soft 90° pulse. A two-dimensional (2D) Fourier transformation followed by a shearing transformation gave a pure absorption mode 2D contour plot [21–23]. The second-order quadrupolar effect (SOQE) and isotropic chemical shift ($\delta_{iso}$) values were calculated according to the procedures in Ref. [21]. $^{29}$Si MAS NMR spectra with high power proton decoupling were recorded at 79.4 kHz using a 7.5-mm MAS probe with a spinning rate of 4 kHz. 4,4-Dimethyl-4-silapentane sulfonate sodium (DSS) was used as the chemical shift reference for $^{29}$Si MAS NMR spectroscopy. A total of 1024 scans were accumulated with a $\pi/4$ pulse width of 2 μs and a 4-s recycle delay. Before the $^1$H MAS NMR measurements, samples were dehydrated at 400 °C at a pressure below $10^{-2}$ Pa for 20 h. $^1$H MAS NMR spectra were collected at 399.9 MHz using a single-pulse sequence with a $\pi/4$ pulse, a 4-s recycle delay, and a spinning speed of 10 kHz. Chemical shifts were referenced to DSS. For the determination of quantitative results, all samples were weighed, and the spectra were calibrated by measuring a known amount of 1,1,1,3,3,3-hexafluoro-2-propanol performed in the same conditions [19]. The Dmfit software was used for deconvolution using fitted Gaussian–Lorentzian line shapes [24].

#### 2.2.3. Hyperpolarized $^{129}$Xe NMR measurements

Continuous-flow hyperpolarized $^{129}$Xe NMR spectra were collected at 110 MHz under static conditions. Optical polarization of xenon was achieved with a home-built pumping cell in the fringe field of the spectrometer magnet and a 60 W dual diode laser array (Coherent Inc.). A flow of 1% Xe–1% $N_2$–98% He gas mixture was delivered to the sample region via plastic tubing. Variable temperature measurements also were performed from room temperature to 153 K. All of the spectra were acquired with a 3.0-μs $\pi/2$ pulse, 200–400 scans, and a 2-s recycle delay. Chemical shifts were referenced to the signal of xenon gas.

### 2.3. Catalyst evaluation

The catalysts (∼2.0 g) were tested in a 10-mm-diameter, fixed-bed flow microreactor [17]. After activation for 1 h at 823 K under nitrogen to remove the moisture, the catalysts were cooled to the reaction temperature at 393 K. The reaction products were analyzed using a Shimadzu GC-8A gas chromatograph with a flame ionization detector. Propene was the main product; trace amounts of $C_5$–$C_{10}$ oligomers also were detected. The conversion of ethene and butene-2 was calculated on the basis of carbon number using methane and butane as the internal standards.

## 3. Results and discussion

### 3.1. XRD patterns and $N_2$ adsorption data

XRD patterns of Mo species loaded on HBeta zeolite with different alumina contents are shown in Fig. 1. It can be seen that the resultant HBeta zeolites have typical BEA structures

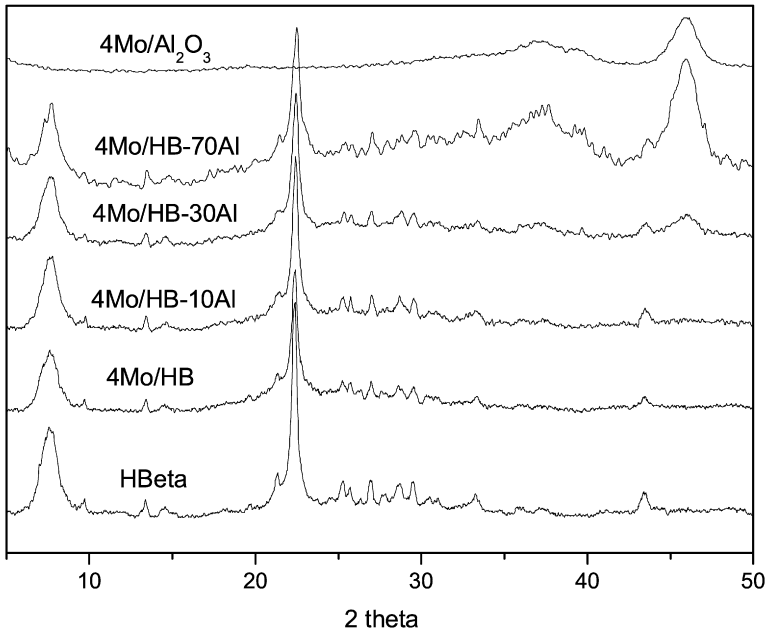


Fig. 1. XRD patterns of HBeta zeolites and 4Mo/HB-*n*Al catalysts.

Table 1
Framework Si/Al ratios, Al contents and relative crystallinity of the HBeta and 4Mo/HB-*n*Al samples

| Sample | HBeta | 4Mo/HB | 4Mo/HB-10Al | 4Mo/HB-30Al | 4Mo/HB-70Al |
|---|---|---|---|---|---|
| Relative crystallinity (%)[a] | 100 | 60 | 72 | 70 | 72 |
| Framework Si/Al ratio[b] | 24 | 34 | 31 | 28 | 28 |
| Framework Al content (μmol $g^{-1}$ (±5%))[c] | 592 | 400 | 455 | 486 | 482 |

[a] Determined by XRD patterns and the intensity of the signal at $2\theta = 22.4°$ was used to evaluate the crystallinity of the Beta zeolites.
[b] Framework Si/Al ratio of HBeta zeolites in the composite support determined by $^{29}$Si MAS NMR.
[c] Framework Al content of HBeta zeolites in the composite support determined by $^{27}$Al MAS NMR using $(NH_4)Al(SO_4)_2 \cdot 12H_2O$ as the external standard.

Table 2
Surface areas and pore volumes of HB-*n*Al supports and 4Mo/HB-*n*Al catalysts

| Sample | HBeta | 4Mo/HB | HB-10Al | 4Mo/HB-10Al | HB-30Al | 4Mo/HB-30Al | HB-70Al | 4Mo/HB-70Al | $Al_2O_3$ | 4Mo/$Al_2O_3$ |
|---|---|---|---|---|---|---|---|---|---|---|
| BET surface area ($m^2$/g support) | 632 | 334 | 589 | 380 | 483 | 384 | 334 | 296 | 223 | 210 |
| Total pore volume (ml/g support) | 0.47 | 0.24 | 0.46 | 0.43 | 0.45 | 0.40 | 0.38 | 0.35 | 0.39 | 0.35 |

and good crystallinity [25]. On loading Mo species, the structure of HBeta zeolites is retained, but their relative crystallinity decreases significantly compared with the parent zeolites. As shown in Table 1, introduction of 4% Mo leads to a crystallinity loss of 40% for HBeta zeolites. Interestingly, 4% Mo loading results in only a 28% decrease in crystallinity after addition of 10% alumina into the support, indicating that alumina in the composite support may protect the HBeta zeolites framework from destruction. In addition, no $\gamma$-$Al_2O_3$ phase is detected in the XRD spectra until its content reaches 30%, and no diffractions of bulk $MoO_3$ can be observed in any sample, indicating that Mo species are highly dispersed on the support.

Table 2 summarizes the BET surface areas and pore volumes of 4Mo/HB-*n*Al samples measured by $N_2$ adsorption. It is found that the parent HBeta zeolites have the largest surface area and pore volume. Introduction of Mo species leads to a significant decrease in the surface area and total pore volume for all supports, with the effect most obvious on the HBeta support. This may be due to the strong interaction between Mo species and HBeta support, which leads to partial dealumination of the framework [17]. It should be noted here that the loss of BET surface area and pore volume on Mo species loaded on HB-*n*Al composite support is not as obvious as that occurring on HBeta support. For example, introduction of 4% Mo species into HBeta support leads to nearly a 50% reduction in the BET surface area. For the 4Mo/HB-30Al catalyst, only a 20% decrease is observed, and the surface area of $\gamma$-$Al_2O_3$ remains relatively unchanged after addition of Mo species. This indicates that addition of alumina may preserve the framework structure of HBeta zeolites.

### 3.2. $^{29}$Si MAS NMR

Fig. 2 shows the $^{29}$Si MAS NMR spectra of the 4Mo/HB-*n*Al catalysts. The lines at −117 and −113 ppm are attributed to the crystallographically inequivalent sites of the $Si(OSi)_4$

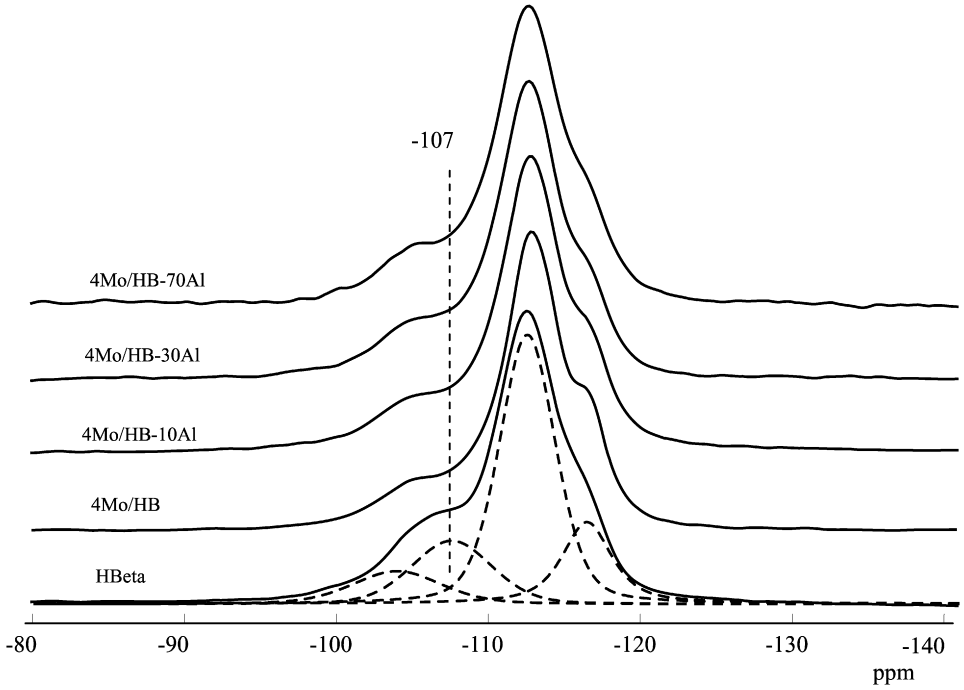


Fig. 2. $^{29}$Si MAS NMR spectra of HBeta zeolites and 4Mo/HB-*n*Al catalysts, which can be deconvoluted using four Gaussian–Lorentzian lines.

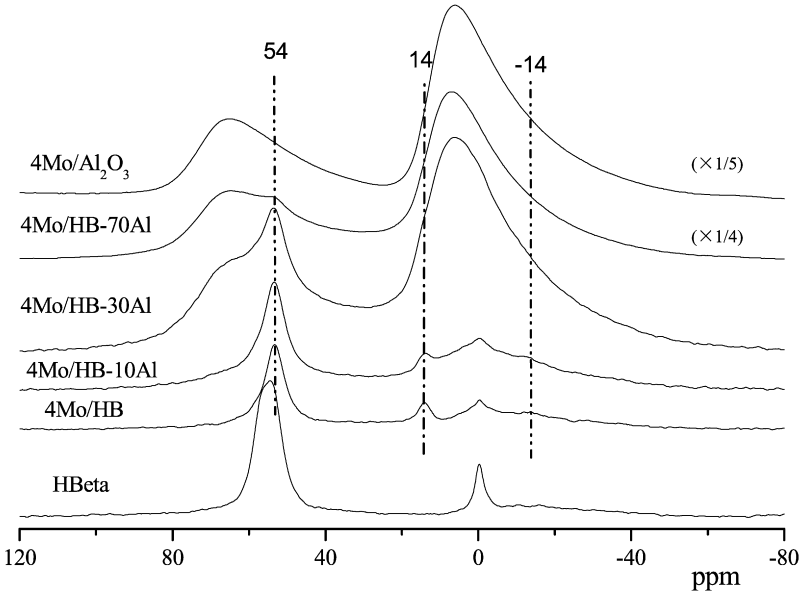


Fig. 3. $^{27}$Al MAS NMR spectra of HBeta zeolites and 4Mo/HB-*n*Al catalysts recorded at a resonance frequency of 104.2 MHz with the sample spinning rate of 15 kHz and 1024 scans. (Prior to measurements, samples were completely hydrated in a desiccator with saturated $NH_4NO_3$ solution.)

groupings in HBeta zeolites. The peak at −107 ppm is supposed to come from the contribution of Si(OAl)(OSi)$_3$ groupings [26]. The peak at −103 ppm is assigned to the silanols with the structure of Si(OSi)$_3$OH because it would be highly enhanced after $^1$H → $^{29}$Si cross-polarization, as shown in our previous study [17]. The framework Si/Al ratios of HBeta zeolites in the composite support can be calculated by deconvolution of the $^{29}$Si MAS NMR spectra. As shown in Table 1, at a fixed Mo loading, the framework Si/Al ratio decreases with increasing alumina content in the support, indicating that addition of alumina into the support may prevent dealumination of the HBeta zeolitic framework. This is in accordance with the above results from $N_2$ adsorption and XRD.

### 3.3. $^{27}$Al MAS and two-dimensional MQ MAS NMR

Fig. 3 illustrates the $^{27}$Al MAS NMR spectra of 4Mo/HB-*n*Al samples. The peaks at about 54 and 0 ppm in spectrum of HBeta zeolites are assigned to the tetrahedrally coordinated framework and octahedrally coordinated extra-framework Al, respectively [27]. In addition, the introduction of Mo species on the support produces two new peaks at −14 and 14 ppm,

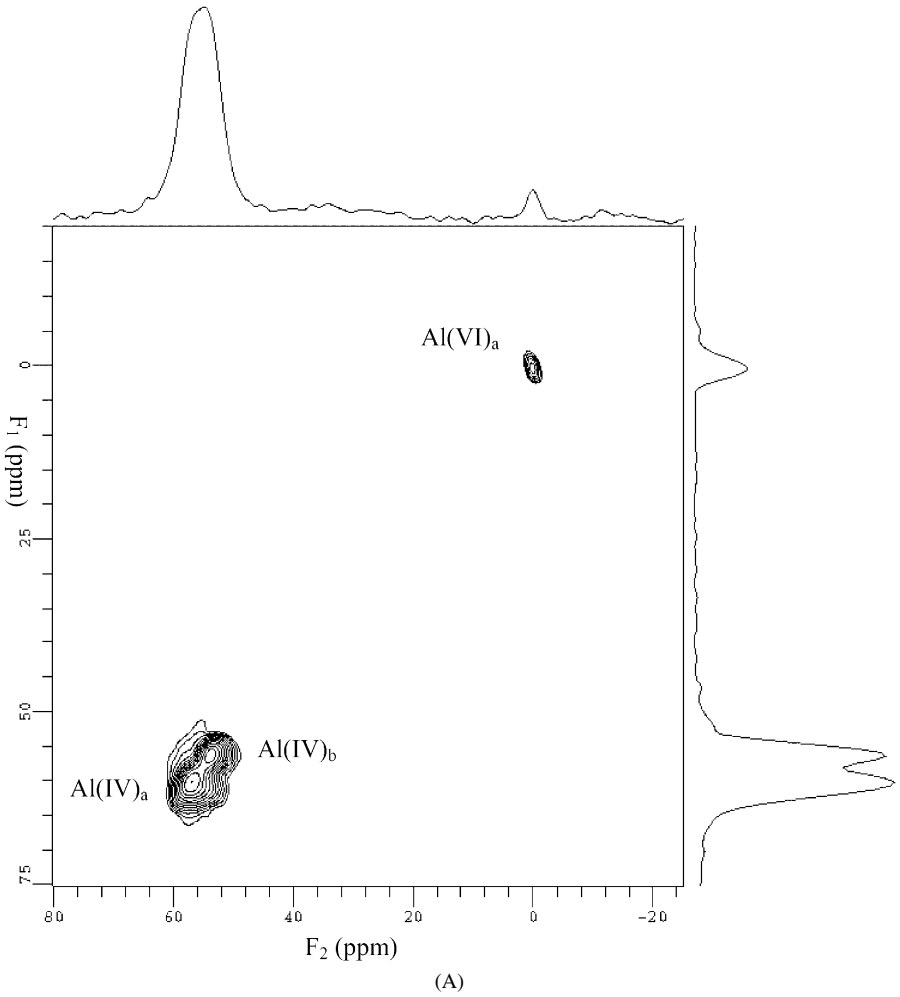


Fig. 4. Two-dimensional $^{27}$Al MQ MAS NMR spectra of samples: (A) HBeta, (B) 4Mo/HB, (C) 4Mo/HB-30Al. The corresponding $^{27}$Al MAS NMR spectrum is given on the top of the MQ MAS plot. The $F_1$ projection is the pure isotropic spectrum. Asterisk denotes the sidebands.

corresponding to the nonhydrated and hydrated forms of the $Al_2(MoO_4)_3$ phase [17,28]. Two broad lines gradually emerge at around 6 and 67 ppm with increasing alumina content in the support; these peaks are assigned to the octahedral and tetrahedral Al in $\gamma$-alumina, respectively [29]. Table 1 shows the quantitative analysis of the framework Al content from $^{27}$Al MAS NMR measurements. The framework Al content of HBeta zeolites decreases from 592 to 400 μmol/g after introduction of Mo species, which means the dealumination of HBeta framework. However, the concentration of framework Al in HBeta zeolites increases to 486 μmol/g after addition of 30% alumina into the support. This indicates that addition of alumina into the support may protect the HBeta framework from destruction.

Two-dimensional $^{27}$Al MQ MAS NMR spectra are used to remove the anisotropic line broadening, allowing identification of species with similar isotropic chemical shifts but different quadrupolar coupling constants. As shown in Fig. 4, the overlapped peaks observed in the $^{27}$Al MAS spectra at 54 ppm are clearly resolved in the MQ MAS spectra for HBeta zeolites. Two distinct framework Al species, designated $Al(IV)_a$ and $Al(IV)_b$, can be seen in the tetrahedral region and a third one, $Al(VI)_a$, is also seen in the octahedral environment at ca. 0 ppm. When HBeta was impregnated with Mo species, the $^{27}$Al MQ MAS spectra of Mo/HBeta reveals an additional species, $Al(IV)_c$, with an isotropic chemical shift ($\delta_{iso}$) at 58.8 ppm along with the line at 14 ppm assigned to a hydrated species of aluminum molybdate, $Al_2(MoO_4)_3$. The signal of $Al(IV)_c$ appears in the resonance region of the tetrahedral aluminum framework and exhibits a large quadrupolar interaction with the SOQE of 4.0 MHz. This large anisotropic quadrupolar broadening makes it difficult to identify in the usual $^{27}$Al MAS NMR spectra, however, it is clearly noticeable in the isotropic $F_1$ projection. At the same time, we note that the intensity of the $Al(IV)_a$ signal is readily decreased from the HBeta framework after impregnation of Mo species. The $Al(IV)_a/Al(IV)_b$ ratio in the framework aluminum content decreases from 0.6 to 0.06. This implies that introduction of Mo species preferentially removes aluminum atoms from crystallographic positions represented by $Al(IV)_a$. In the meantime two new peaks of $Al(IV)_c$ and $Al(VI)_b$ can be seen in the spectra. Consequently, it is the introduction of Mo species that leads to formation of a third framework $Al(IV)_c$ species and the subsequent appearance of nonframework $Al_2(MoO_4)_3$. This suggests that the Al atoms corresponding to peak $Al(IV)_c$ can be assigned to

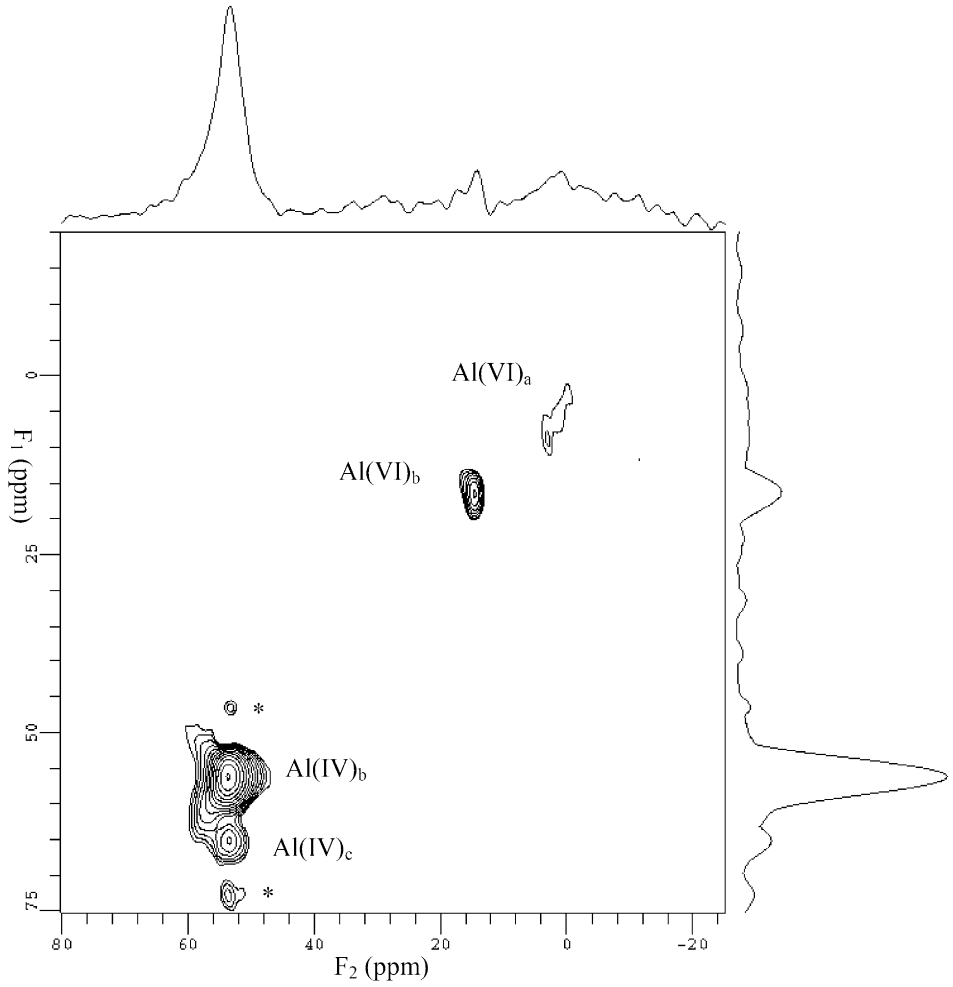


(B)

Fig. 4. (*continued*)

the distorted extra-framework tetrahedral aluminum, similar to the findings reported by van Bokhoven et al. in the hydrothermal treatment of HBeta zeolites [30,31]. For the 4Mo/HB-30Al catalyst, along with the tetrahedral $Al(IV)_d$ in alumina, some $Al(IV)_a$ can be seen in the HBeta framework, with an increase in $Al(IV)_a/Al(IV)_b$ ratio from 0.06 to 0.23. At the same time, the peak belonging to the distorted tetrahedral $Al(IV)_c$ is not so evident as that in the 4Mo/HB catalyst. It exhibits a smaller quadrupolar interaction ($\delta_{iso} = 58.3$ ppm, SOQE = 3.2 MHz). Therefore, alumina can protect the specific T-sites in the framework of HBeta zeolites when impregnating Mo species. The framework aluminum in HBeta zeolites can remain at the same crystallographic sites after addition of alumina into the support.

### 3.4. Hyperpolarized $^{129}Xe$ NMR

$^{129}Xe$ NMR spectroscopy is a powerful tool for characterizing the porous structure and location of guest species in materials [32]. Its main advantage is the high sensitivity of the chemical shift of $^{129}Xe$ to its local environments. However, the application of thermally polarized $^{129}Xe$ NMR to materials is often hampered by a relatively weak signal-to-noise ratio and long relaxation time, especially for the mesoporous materials [33]. An increase in sensitivity of several orders of magnitude can be achieved using laser polarization techniques to produce hyperpolarized xenon [34–36]. Fig. 5 shows the hyperpolarized $^{129}Xe$ NMR spectra of Mo/HB-*n*Al samples acquired at different temperatures. The hyperpolarized $^{129}Xe$ NMR spectrum acquired for HBeta zeolites at room temperature shows a peak at 80 ppm in addition to the xenon gas signal at 0 ppm (see Fig. 5A). The former peak is characteristic of xenon adsorbed in the 12-membered ring channels of HBeta [37,38]. There is no signal for xenon adsorbed in pure alumina at room temperature; however, when the measurement temperature drops to 173 K, a signal at about 103 ppm can be seen, which can be assigned to xenon adsorbed in the pores of alumina [39]. For the HBeta–$Al_2O_3$ composite support, only the peak at 80 ppm corresponding to xenon in the HBeta pores is detectable. This may be due to the preferential adsorption of xenon in the micropores rather than in the mesopores [32]. After introduction of Mo species, a small downfield shift of xenon signal in HBeta zeolites is observed at lower temperatures (see Figs. 5B and 5C). This indicates that a very small portion of Mo species is deposited into the pores of HBeta, slightly narrowing the pore size of HBeta. At the same time, a small peak at ca. 103 ppm

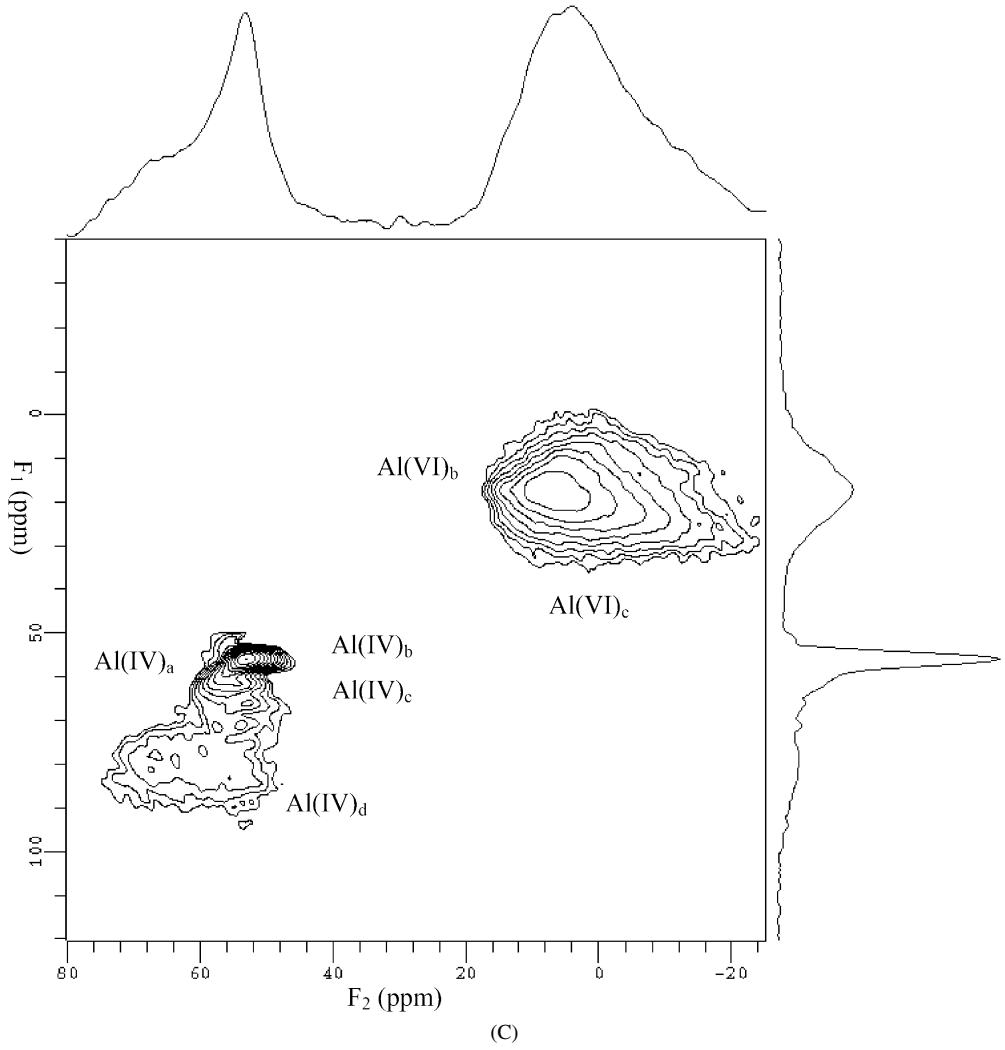


(C)

Fig. 4. (*continued*)

emerges on Mo loading, which is consistent with the signal from the empty alumina. This peak becomes more evident and shifts to the lower field when the temperature decreases down to 153 K for the HBeta–$Al_2O_3$ composite supported with 4 or 9 wt% Mo. However, the signal from the empty alumina is absent in the $^{129}$Xe NMR spectra of HBeta–$Al_2O_3$ composite support. This demonstrates that addition of Mo species into the composite support may inhibit the exchange of xenon gas in the HBeta and alumina domains, and thus Mo species may locate at the boundary of the HBeta and alumina. At a Mo loading as high as 9 wt%, an additional peak is centered at ca. 145 ppm along with the peak of xenon in the empty alumina at 131 ppm. This peak can be ascribed to the xenon adsorbed in the alumina with Mo species, because the deposition of Mo species into the pores of alumina may decrease the average free path of xenon in alumina, leading to a low-field shift of the xenon signal [32]. Thus, the hyperpolarized $^{129}$Xe NMR measurements clearly show that the distribution of Mo species is heterogeneous in the HBeta zeolites and alumina composite support. These species are deposited more at the boundary and in the pores of alumina than in the pores of HBeta zeolites at higher Mo loadings.

### *3.5. SEM and TEM images*

The morphology and distribution of Mo species in HBeta and alumina composite support were further investigated by high-resolution SEM and TEM. Fig. 6A shows the SEM image of the 4Mo/HB-30Al sample, showing the HBeta particles surrounded by irregular alumina floccules. Table 3 gives the quantitative analysis of the components by X-ray EDS, demonstrating the concentrations of Al and Mo elements are higher in site I than in site II. Therefore, Mo species are distributed more in the alumina than in the HBeta zeolites. This finding is verified by the TEM images. Fig. 6B presents a cross-sectional TEM image of the 4Mo/HBeta-30Al sample, showing a clear boundary between site aa and site bb. Quantitative EDS measurement shows that site bb has a much higher Al content than site aa (see Table 3); thus, site bb should be associated with alumina, whereas site aa corresponds to HBeta zeolites. The concentration of Mo elements is higher in alumina than in HBeta zeolites, indicating that Mo species are preferentially distributed in alumina rather than in HBeta zeolites, which is consistent with the above results from hyperpolarized $^{129}$Xe NMR. This phenomena was also observed by Li et al. in Ni–Mo sulfide catalysts

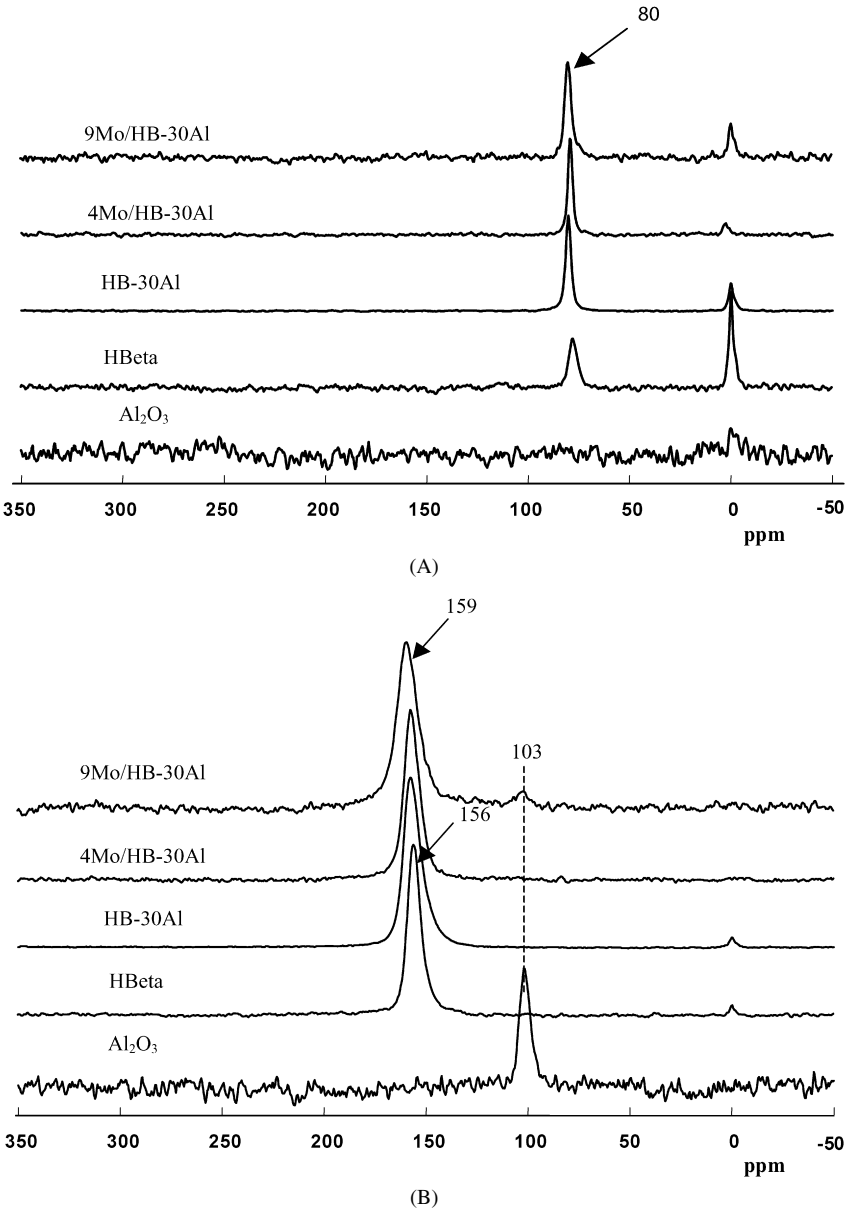


Fig. 5. Variable-temperature hyperpolarized $^{129}$Xe NMR spectra of HBeta zeolites, alumina, and Mo/HB-*n*Al catalysts acquired at different temperatures: (A) 293 K, (B) 173 K, (C) 153 K.

supported on mixed USY zeolites and alumina for hydrotreatment [40].

### 3.6. $^{1}$H MAS NMR

High-resolution $^{1}$H MAS NMR is a powerful and direct method for characterizing the acidic sites in solid catalysts. Compared with IR, it can provide quantitative information on the hydroxyl species without the problem of extinction coefficients [41]. Fig. 7 shows the $^{1}$H MAS NMR spectra of 4Mo/HB-*n*Al catalysts. Two broad peaks can be seen on the 4Mo/$Al_2O_3$ sample. The line at about −0.2 ppm is assigned to the basic hydroxyls on alumina, and the line centered at ca. 2.2 ppm belongs to the acidic hydroxyls [42]. In addition, three peaks at about 0.8, 1.7, and 2.3 ppm can be differentiated on HBeta zeolites, which are attributed, respectively, to the nonacidic unperturbed extra-framework aluminum hydroxyls, silanol groups, and Al–OH experiencing hydrogen bonds with neighboring oxygen atoms. The peak at 3.9 ppm should be assigned to the bridging hydroxyl groups, i.e. Brønsted acidic sites [41]. The broad line centered at 5.1 ppm also can be seen in the deconvoluted spectra, which may be attributed to a second Brønsted acidic site interacting electrostatically with the zeolite framework because it could be significantly suppressed after Al irradiation [17]. Quantitative analysis of the spectra demonstrates that introduction of 4% Mo leads to the consumption of Brønsted acid sites from 228 to 127 μmol/g of the support, likely due to the strong interaction between the Mo species and the HBeta zeolites [17]. When alumina is incorporated into the support, more Brønsted acid sites (i.e., 151 μmol/g) are preserved on the 4Mo/HB-30Al catalyst. This is in agreement

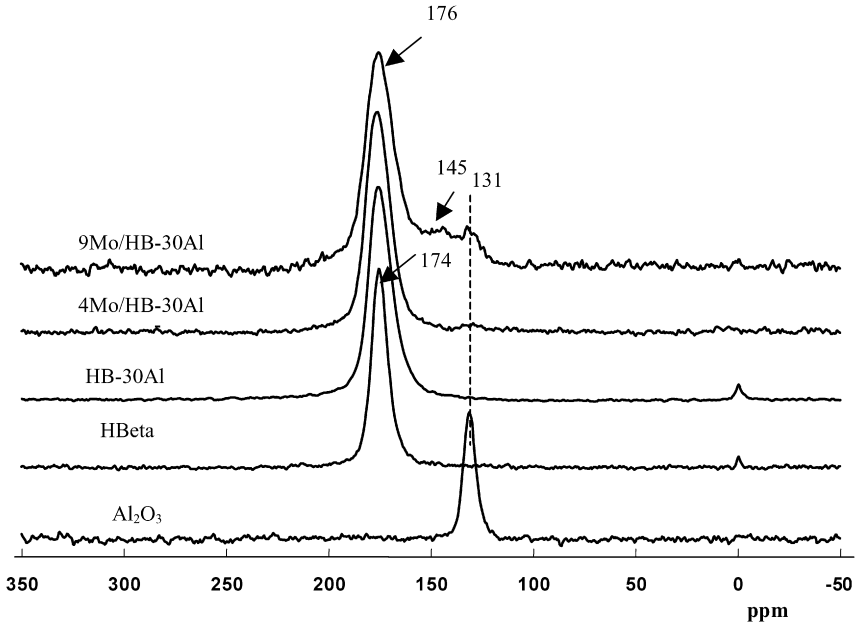


(C)

Fig. 5. (*continued*)

Table 3
Chemical compositions of different parts in 4Mo/HB-30Al catalyst detected by energy dispersive spectroscopy (EDS)

| Element | I (molar fraction%) | II (molar fraction%) | bb (molar fraction%) | aa (molar fraction%) |
|---|---|---|---|---|
| O | 63.1 | 63.5 | 65.9 | 67.2 |
| Al | 20.2 | 10.4 | 24.8 | 3.2 |
| Si | 16.1 | 25.7 | 8.2 | 29.2 |
| Mo | 0.6 | 0.4 | 1.1 | 0.4 |

with the above $^{27}$Al MQ MAS NMR results in which more tetrahedral aluminum remained in the framework of 4Mo/HB-30Al compared with 4Mo/HBeta. Further increasing the alumina content in the support to 70% decreases the concentration of Brønsted acid sites to ca. 90 μmol/g, due mainly to the lower content of HBeta in the support.

### *3.7. Catalytic performance of cross-metathesis of ethene and butene-2 to propene*

Fig. 8 illustrates the catalytic performance of olefin metathesis on 4Mo/HBeta-*n*Al catalysts as a function of alumina content. Mo supported on HBeta zeolites clearly shows the worst performance, with butene-2 conversion of <20% and propene selectivity of ca. 15%. Addition of alumina in the support (e.g., 4Mo/HBeta-10Al) produces significantly improved catalytic performance. As the alumina content is increased, the catalytic activity increases accordingly. At an alumina content of 30–50 wt%, the 4Mo/HB-30Al catalyst shows the highest metathesis activity. Under these conditions, the butene-2 conversion is up to 80%, and the propene selectivity is about 95%. These catalysts also have high stability, with no obvious deactivation after 7 h. Further increases in alumina content (e.g., 4Mo/HBeta-70Al) lead to decreased catalyst activity, however. The conversion of butene-2 is only 35% for Mo loaded on pure alumina support. Clearly, the changes in catalytic activity are related to the structure and property of the support.

Comparing the results from solid-state NMR and SEM/TEM studies with the above catalytic performance of Mo/HBeta–$Al_2O_3$ seems to show that addition of $\gamma$-alumina into the support protects the framework of HBeta zeolites from destruction. In addition, the preferential migration of Mo species into the alumina pores may preserve the aluminum atoms at specific T-positions in HBeta zeolites. This may result in the moderate distribution of Mo species and also a proper acidity of the support, as evidenced by $^{1}$H MAS NMR spectra. Combined with catalytic performance data, this may indicate that Brønsted acidic sites are involved in the metathesis reaction. This is consistent with the results from Mol et al. [43–45], who also observed a correlation between metathesis activity and Brønsted acidic sites on $Re_2O_7/Al_2O_3$ catalysts. We suspect that the dispersion of Mo species and addition of alumina into the support, as well as the proper acidity, may be advantageous for the metathesis of ethene and butene-2 to propene.

## 4. Conclusion

4Mo/HBeta–30%$Al_2O_3$ catalyst demonstrates much better performance for the metathesis of ethene and butene-2 to propene compared with the catalyst without alumina in the support. XRD, $N_2$ adsorption, and solid-state MAS NMR results

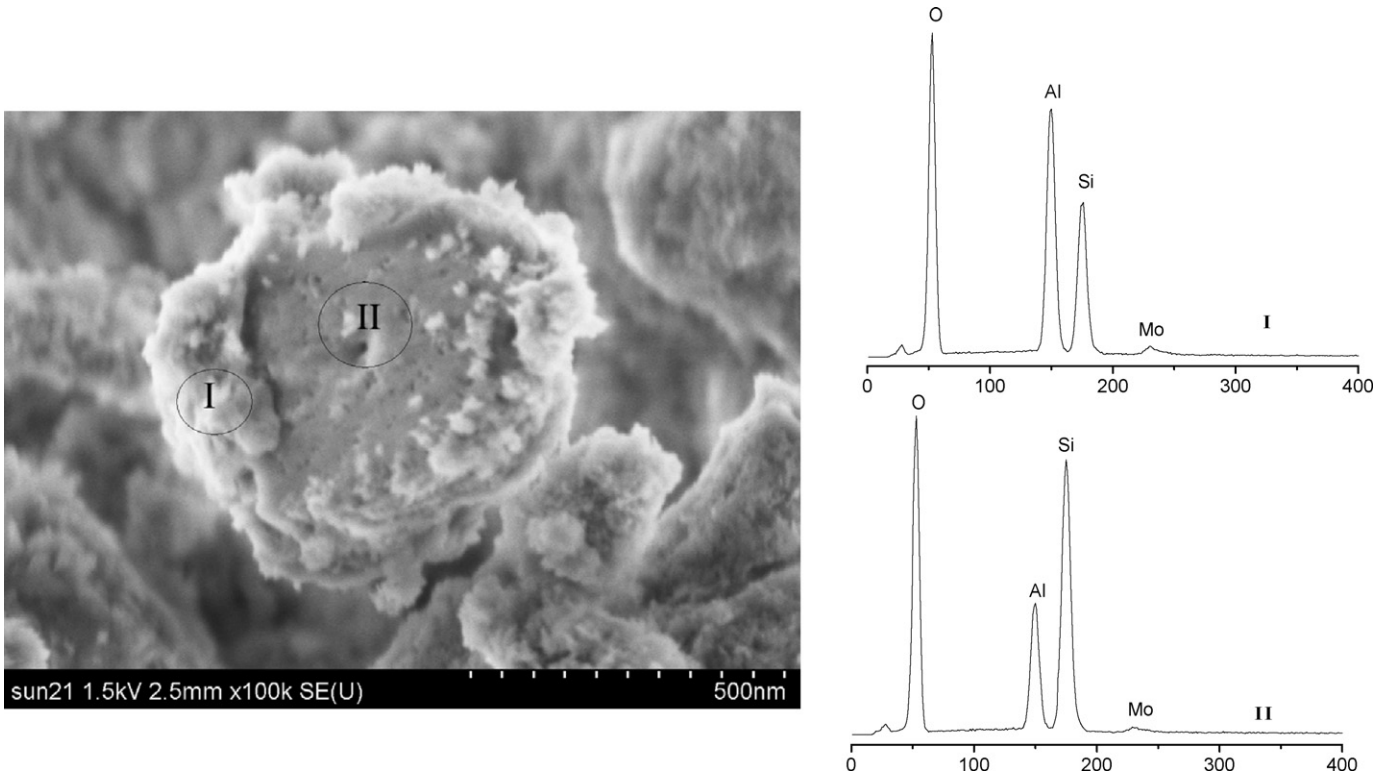


(A)

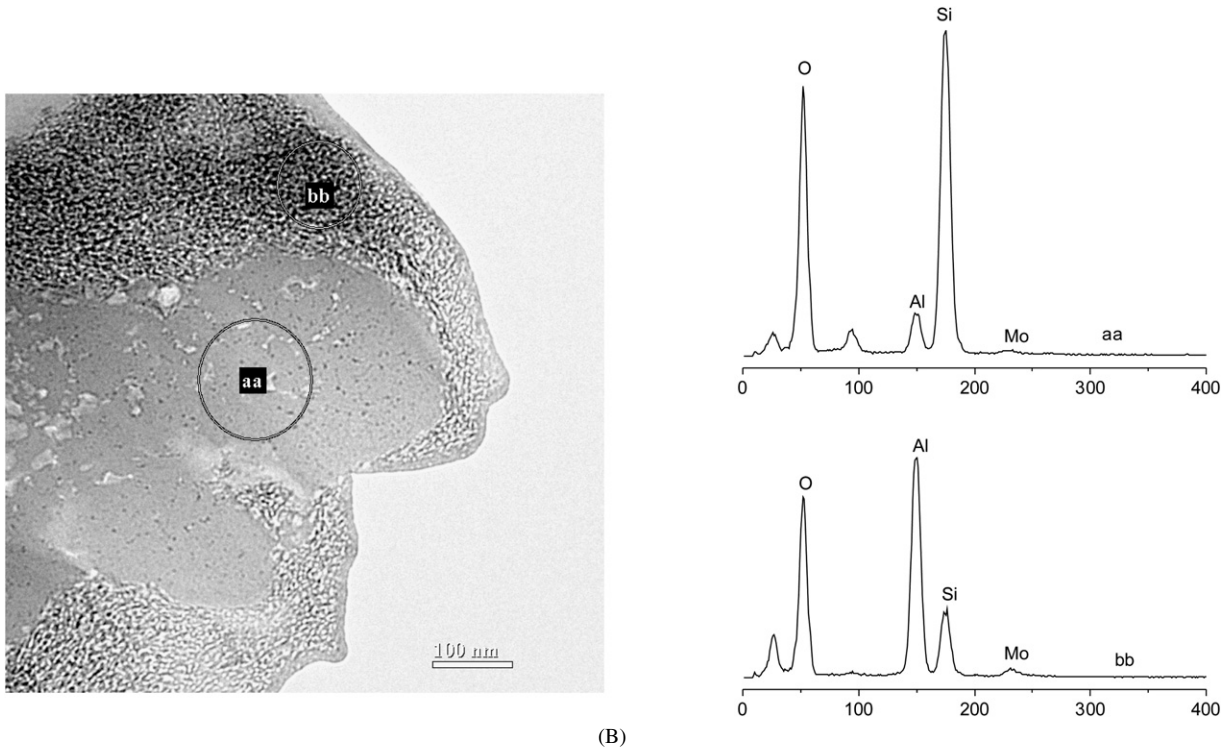


(B)

Fig. 6. SEM (A), cross-sectional TEM (B) images, and EDS analysis of 4Mo/HB-30Al catalyst.

demonstrate that the addition of $Al_2O_3$ into the support protects the framework of HBeta zeolites from destruction. Hyperpolarized $^{129}$Xe NMR, SEM, and TEM images indicate that Mo species are dispersed more in the alumina than in the HBeta zeolites. Such a distribution may preserve the aluminum atoms at specific T-positions in HBeta zeolites, as evidenced by $^{27}$Al MQ MAS NMR, and result in the moderate distribution of Mo species and acidity in the composite support. These effects may contribute to the good performance of Mo/HBeta–$Al_2O_3$ catalysts in olefin metathesis.

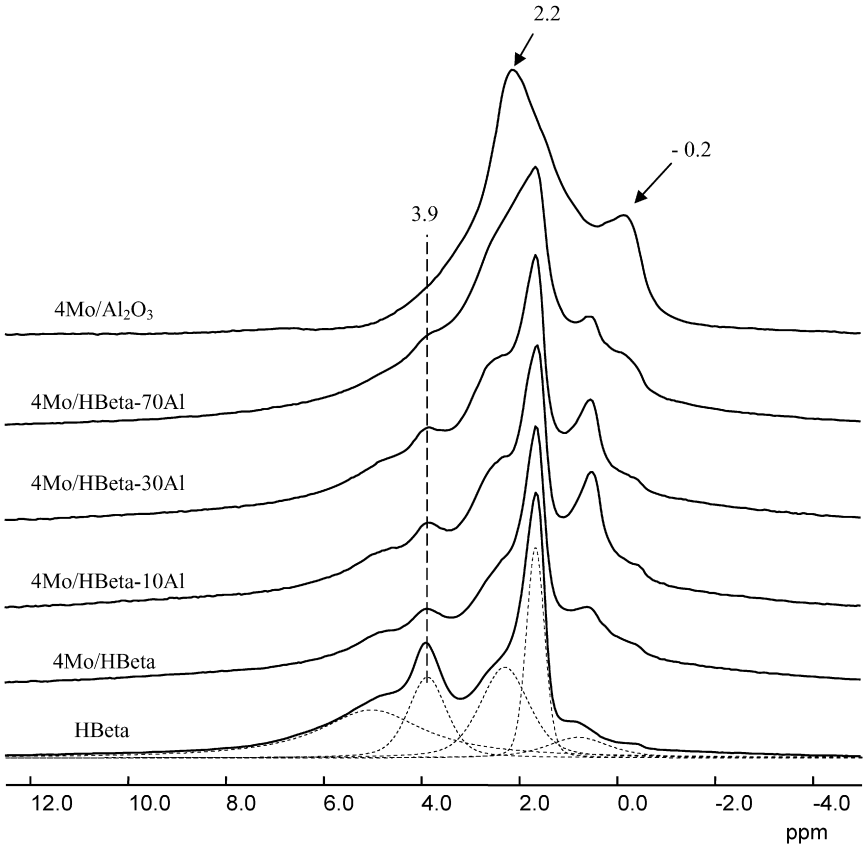


Fig. 7. $^{1}$H MAS NMR spectra of 4Mo/HB-*n*Al catalysts. The spinning rate was 10 kHz, and 200 single-pulse scans were accumulated.

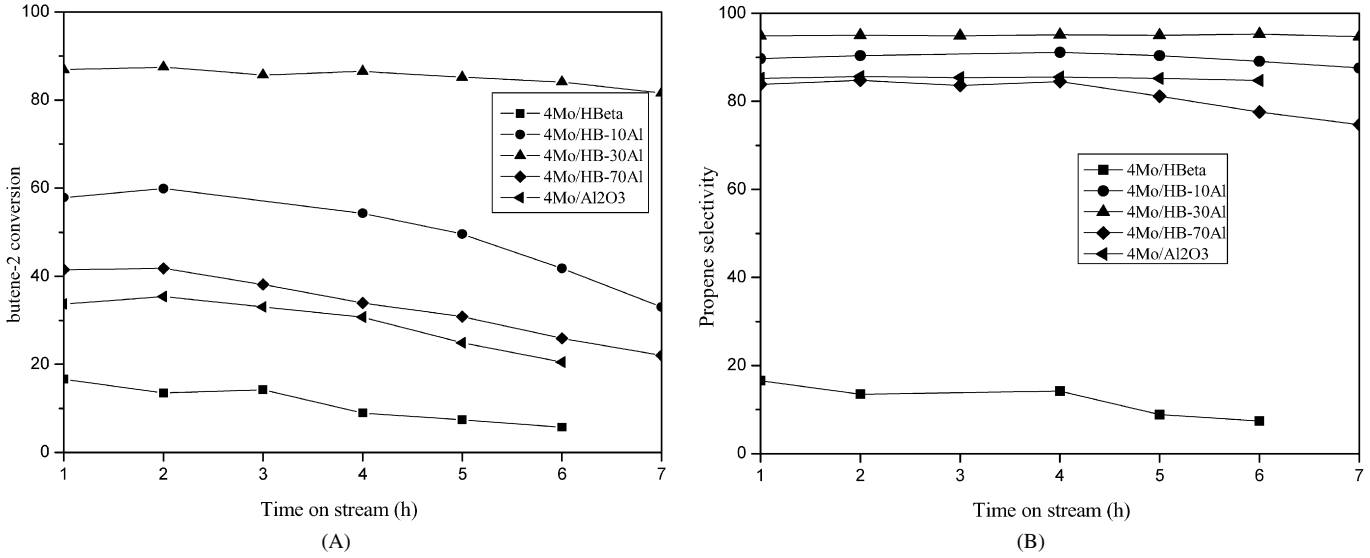


Fig. 8. Catalytic conversions (A) and selectivities (B) of 4Mo/HB-*n*Al catalysts with different alumina contents in the metathesis of ethene and butene-2 to propene (reaction temperature: 393 K, pressure: 1.0 MPa, ethene/2-butene = 3:1, WHSV of ethene: 1.2 $h^{-1}$).

## Acknowledgments

Financial support was provided by the National Natural Science Foundation of China (grants 20403017 and 20303019) and the Ministry of Science and Technology of China through the National Key Project of Fundamental Research (grant 2003CB615806). The authors thank Dr. J.M. Sun (DICP) and Dr. D. Su (Fritz-Haber Institute, Germany) for help with the SEM and TEM measurements and the anonymous reviewers for their helpful discussions and suggestions.

## References

[1] Y. Chauvin, Angew. Chem. Int. Ed. 45 (2006) 3741.
[2] R.R. Schrock, Angew. Chem. Int. Ed. 45 (2006) 3748.

[3] R.H. Grubbs, S.J. Miller, G.C. Fu, Acc. Chem. Res. 28 (1995) 446.
[4] K.J. Ivin, J.C. Mol, Olefin Metathesis and Metathesis Polymerization, Academic Press, San Diego, 1997, p. 397.
[5] J.C. Mol, J. Mol. Catal. A 213 (2004) 39.
[6] J.C. Mol, Catal. Today 51 (1999) 289.
[7] R. Hamtil, N. Žilková, H. Balcar, J. Čejka, Appl. Catal. A 302 (2006) 193.
[8] A.M.J. Rost, H. Schneider, J.P. Zoller, W.A. Herrmann, F.E. Kühn, J. Organomet. Chem. 690 (2005) 4712.
[9] M. Sibeijn, J.C. Mol, Appl. Catal. 67 (1991) 279.
[10] X. Xu, C. Boelhouwer, J.I. Benecke, D. Vonk, J.C. Mol, J. Chem. Soc. Faraday Trans. 82 (1986) 1945.
[11] F.C. Sheu, C.T. Hong, W.L. Hwang, C.J. Shih, J.C. Wu, C.T. Yeh, Catal. Lett. 14 (1992) 297.
[12] M. Sibeijn, R. Spronk, J.A.R. van Veen, J.C. Mol, Catal. Lett. 8 (1991) 201.
[13] R. Spronk, J.A.R. van Veen, J.C. Mol, J. Catal. 144 (1994) 72.
[14] W. Grunert, R. Feldhaus, K. Anders, E.S. Shpiro, K.H.M. Minachev, J. Catal. 120 (1989) 444.
[15] C.V. Schalkwyk, A. Spamer, D.J. Moodley, T. Dube, J. Reynhardt, J.M. Botha, Appl. Catal. A 255 (2003) 121.
[16] S.L. Liu, S.J. Huang, W.J. Xin, J. Bai, S.J. Xie, L.Y. Xu, Catal. Today 93–95 (2004) 471.
[17] X.J. Li, W.P. Zhang, S.L. Liu, X.W. Han, L.Y. Xu, X.H. Bao, J. Mol. Catal. A 250 (2006) 94.
[18] H. Kraus, R. Prins, J. Catal. 164 (1996) 260.
[19] M. Müller, G. Harvey, R. Prins, Microporous Mesoporous Mater. 34 (2000) 281.
[20] J.P. Amoureux, C. Fernandez, S. Steuernagel, J. Magn. Reson. 123 (1996) 116.
[21] M.E. Simth, E.R.H. van Eck, Prog. Nucl. Magn. Reson. Spectrosc. 34 (1999) 159.
[22] J. Rocha, C.M. Morais, C. Fernandez, Top. Curr. Chem. 246 (2004) 141.
[23] A. Medek, J.S. Harwood, L. Frydman, J. Am. Chem. Soc. 117 (1995) 12779.
[24] D. Massiot, F. Fayon, M. Capron, I. King, S. LeCalvé, B. Alonso, J.O. Durand, B. Bujoli, Z. Gan, G. Hoatson, Magn. Reson. Chem. 40 (2002) 70.
[25] M.J. Eapen, K.S.N. Reddy, V.P. Shiralkar, Zeolites 14 (1994) 295.
[26] J. Perez-Pariente, J. Sanz, V. Fornes, A. Corma, J. Catal. 124 (1990) 217.
[27] J.A. van Bokhoven, D.C. Koningsberger, P. Kunkeler, A.P.M. Kentgens, J. Am. Chem. Soc. 122 (2000) 12842.
[28] W.P. Zhang, D. Ma, X.W. Han, X.M. Liu, X.H. Bao, X.W. Guo, X.S. Wang, J. Catal. 188 (1999) 393.
[29] H. Kraus, M. Müller, R. Prins, J. Phys. Chem. B 102 (1998) 3862.
[30] A. Omegna, M. Vasic, J.A. van Bokhoven, G. Pringruber, R. Prins, Phys. Chem. Chem. Phys. 6 (2004) 447.
[31] A. Abraham, S.H. Lee, C.H. Shin, S.B. Hong, R. Prins, J.A. van Bokhoven, Phys. Chem. Chem. Phys. 6 (2004) 3031.
[32] J.L. Bonardet, J. Fraissard, A. Gedeon, M.A. Springuel-Huet, Catal. Rev. Sci. Eng. 41 (1999) 115.
[33] T. Pietrass, J.M. Kneller, R.A. Assink, M.T. Anderson, J. Phys. Chem. B 103 (1999) 8837.
[34] M. Haake, A. Pines, J.A. Reimer, R. Seydoux, J. Am. Chem. Soc. 119 (1997) 11711.
[35] I.L. Moudrakovski, A. Nossov, S. Lang, S.R. Breeze, C.I. Ratcliffe, B. Simard, G. Santyr, J.A. Ripmeester, Chem. Mater. 12 (2000) 1181.
[36] W.P. Zhang, C.I. Ratcliffe, I.L. Moudrakovski, J.A. Ripmeester, Anal. Chem. 77 (2005) 3379.
[37] S.B. Liu, J.F. Wu, L.J. Ma, T.C. Tsai, I. Wang, J. Catal. 132 (1991) 432.
[38] Q.J. Chen, J.L. Guth, A. Seive, P. Caullet, J. Fraissard, Zeolites 11 (1991) 798.
[39] K. Hagiwara, T. Ebihara, N. Urasato, T. Fujikawa, Appl. Catal. A 285 (2005) 132.
[40] D. Li, A. Nishijima, D.E. Morris, G.D. Guthrie, J. Catal. 188 (1999) 111.
[41] M. Hunger, Catal. Rev. Sci. Eng. 39 (1997) 345.
[42] W.P. Zhang, M.Y. Sun, R. Prins, J. Phys. Chem. B 106 (2002) 11805.
[43] X. Xu, J.C. Mol, C. Boelhouwer, J. Chem. Soc. Faraday Trans. 82 (1986) 2707.
[44] A. Andreini, X. Xu, J.C. Mol, Appl. Catal. 27 (1986) 31.
[45] A. Andreini, J. Mol. Catal. 65 (1991) 359.